Nanopatterning effects on magnetic anisotropy of epitaxial Fe(001) micrometric squares

D. Jaque
Departamento de Física de Materiales, CC. Físicas, Universidad Complutense, Av. Complutense, 28040 Madrid, Spain

J. I. Martín
Departamento de Física, Facultad de Ciencias, Universidad de Oviedo, 33007 Oviedo, Spain

G. Armelles, J. L. Costa-Krämer, and F. Briones
Instituto de Microelectrónica de Madrid, CNM, CSIC, Isaac Newton 8, PTM Tres Cantos, 28760 Madrid, Spain

J. L. Vicent[a)]
Departamento de Física de Materiales, CC. Físicas, Universidad Complutense, Av. Complutense, 28040 Madrid, Spain

(Received 21 June 2001; accepted for publication 27 September 2001)

Magneto-optic (MO) studies are performed on regular arrays of Fe(100) micrometric squares, where the elements are patterned with different sizes (2.5–10 μm) and separations (0.2–0.6 μm). When a laser beam is focused inside the patterned structure a Bragg diffraction pattern is produced allowing MO studies on both reflected and diffracted spots. The magnetic anisotropy has been analyzed by in-plane MO hysteresis loops finding that, for square sizes below 2.5 μm, it is not consistent with the Fe crystalline cubic anisotropy, presenting a uniaxial-like behavior. The magnitude of the corresponding anisotropy constants has been determined by analyzing the array response (on reflected and diffracted spots) to a rotational magnetic field in a magneto-optical torque setup. For square sizes of 10 μm the anisotropy induced by patterning is negligible whereas for the small squares (2.5 μm) the uniaxial magnetic constant has been found to be roughly 0.2 times the Fe cubic anisotropy constant. © *2002 American Institute of Physics*. [DOI: 10.1063/1.1421042]

I. INTRODUCTION

The fast development of lithography techniques during the last few years makes it possible to produce periodic arrays of magnetic elements with submicrometric dimensions.[1] These techniques provide full control over the size, period, and symmetry of the microstructures. The potential technological interest extends from data storage devices to integrated magnetoelectronic devices.[2,3] On the other hand, these patterned arrays are of great relevance from the basic point of view since fundamental properties of mesoscopic magnetism can be probed. As an example, the correlation of magnetic properties of patterned structures with the size and shape of a single element, as well as with the array spacing, is a central issue that is still not fully understood. In particular, the characteristics of the magnetic anisotropy can be controlled and modified at these small scales by changing the geometry and size of the structures. This is a problem of fundamental interest, as magnetic anisotropy is the basis of the magnetization reversal processes that take place in the material.

In this work we have studied the magnetic anisotropy of arrays of single crystalline Fe(001) squares separated by submicrometric distances. A systematic investigation of the magneto-optical (MO) properties has been performed by a combination of conventional MO Kerr effect (MOKE) measurements and MO torque (MOT) experiments.[4]

In a first step, the measurements of the MOKE hysteresis loops as a function of sample orientation have been used to determine the distribution of magnetic easy axes as a function of the square size and separation. Then, the MOT technique has been applied to determine the corresponding anisotropy constants of the patterned structures. By measuring both the reflected (specular measurements) and diffracted (nonspecular measurements) spots generated under laser illumination, MOT has also allowed us to get information about the magnetization distribution state within a single element; this information is usually obtained by magnetic force microscopy (MFM)[5] and by Bitter decoration experiments.[6] In our case we have determined the minimum magnetic field value which ensures a homogeneous magnetization for every direction in a rotating magnetic field configuration.

II. EXPERIMENT

The arrays of magnetic elements were fabricated by patterning single crystal iron films. The deposition of the continuous 200 Å thick Fe film was performed on GaAs substrates with a MgO (001) buffer layer in a triode sputtering system with a base pressure in the low 10^{-9} mbar range. The crystallinity and interfaces of the films are excellent with well-defined peaks in the reflection high-energy electron dif-

a)Electronic mail: jlvicent@fis.ucm.es

fraction and high/low angle x-ray diffraction patterns.[7] To protect them from oxidation, the Fe films are covered *in situ* with a sputtered layer of Pt with a typical thickness of 70 Å.

The patterning of the continuous film was carried out by conventional electron-beam lithography as described elsewhere.[8] Briefly, the as-deposited film is covered by a thin poly-methylmethacrylate (PMMA) film, which is subsequently irradiated in a scanning electron microscope and developed. This PMMA layer is used as a mask during an ion beam etching procedure using Ar ions. Typically, we introduced about 25% overetching in order to ensure that the continuous film was effectively separated. The total patterned area is $500\times500\ \mu m^2$, and the lithographed array of Fe squares present periods (L, defined as the distance between neighbor square centers) of 2.5, 5, and 10 μm and square-square separations (s, defined as the distance between neighbor edges) of 0.2 and 0.6 μm. All the tilings studied in the present work have the square edges parallel to the Fe [110] directions, i.e., directions that are magnetically hard. Atomic force microscopy (AFM) characterization of the fabricated structures is carried out in a commercial Park Scientific unit.

The magnetic anisotropy of the samples has been analyzed by a combination of MOT and MOKE experiments.[4,9] The optical setup was the same for both techniques. The laser (He–Ne) beam is focused on the sample producing a spot size of about 250 μm diameter. The reflected/diffracted p-polarized light is focused inside a Si photodiode. The signal from the photodiode is compensated from the dc offset and amplified. For MOKE experiments the sample is placed inside a Helmholtz coil providing a maximum field of ~400 Oe perpendicular to the incidence plane.

For the MOT measurement the coil is substituted by a magnet mounted on a rotational stage driven by an electrical motor. The rotation frequency can be changed between 10 and 40 Hz. The magnitude of the applied magnetic field at the sample position is controlled by adjusting the distance between the sample and rotating magnet. This control over the applied magnetic field magnitude is necessary since one of the requirements to be satisfied by the MOT data analysis is that the magnitude of the applied magnetic field should be high enough to induce a uniform magnetization in each element in every direction.[4] The reflectivity signal is periodic, with a period that coincides with the inverse of the rotating magnet frequency. The angle of the rotating applied field with respect to the plane of incidence and the applied magnetic field magnitude is measured with a Hall probe. This technique has emerged as a powerful and versatile tool to quantify magnetic anisotropies in unpatterned and patterned films, and it has been successfully applied to determine the anisotropy constants of submicrometric stripe shaped Fe(001) elements.[4]

As was mentioned before, MO measurements have been performed on both diffracted and reflected beams. In the following we classify the diffracted spots in two groups: those that lie in the plane defined by the incident and refracted laser beams are labeled as ''horizontal orders.'' On the other hand those that align perpendicular to this plane are referred to as ''vertical orders.'' In order to clarify this nomenclature

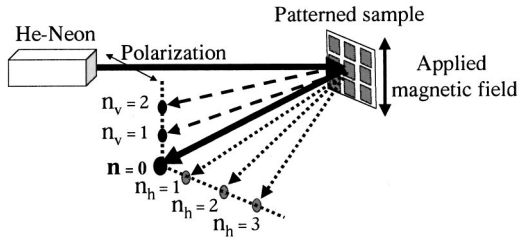

FIG. 1. Schematic drawing of the spatial distribution of diffracted beams with respect to sample orientation and pump laser beam.

Fig. 1 shows a sketch of the spatial distribution of diffracted beams with respect to sample orientation and pump laser beam. In this figure n_h and n_v denote horizontal and vertical orders, respectively. It should be noted that the magnetic field arrangement displayed in Fig. 1 corresponds to that used in MOKE experiments. When MOT measurements are to be performed this magnetic field geometry is substituted by a rotating magnet so that the applied magnetic field is always parallel to the sample surface.

III. RESULTS AND DISCUSSION

A. Determination of magnetic axes distribution

In order to investigate the magnetic anisotropies induced by patterning we have measured in-plane hysteresis loops for different sample orientations. The sample was rotated so that the angle between applied magnetic field and square diagonal was varied from 0° up to 360°. These measurements were performed on both Fe continuous film and also on the square patterned arrays. The angular dependence of the reduced remanence M_r/M_s (M_s being the saturation magnetization and M_r the magnetization at remanence) obtained for the Fe continuous film (not shown) has a well-defined cubic biaxial anisotropy as expected.[7,10]

Figure 2 shows the polar plots of reduced remanence obtained for the patterned arrays as a function of array period (L) and square-square separation (s). Two markedly different behaviors are observed as a function of the square size.

(1) $L=10$ and 5 μm squares. The remanence shows cubic biaxial anisotropy for the two edge distances. This was nevertheless expected since the Fe easy axis extends parallel

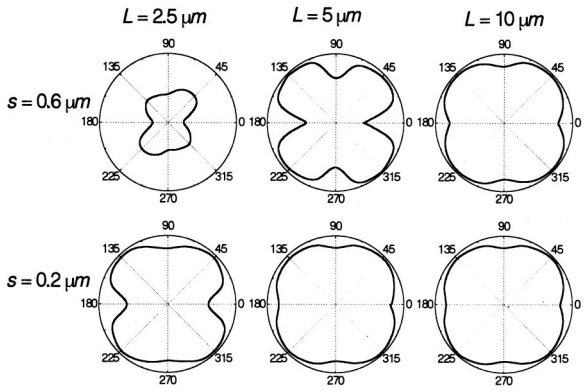

FIG. 2. Polar plots of reduced remanence obtained from the different square arrays.

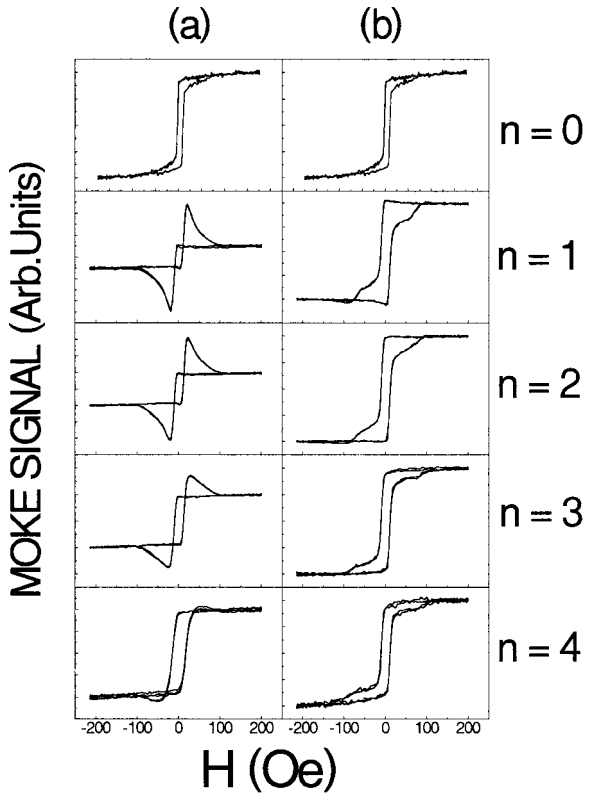

FIG. 3. MO loops obtained in the reflected and diffracted spots. Column (a) displays horizontal diffracted beams whereas vertical orders are shown in column (b).

to the square diagonal so that the net anisotropy is a combination of two cubic anisotropies aligned (Fe and shape anisotropies).

(2) For the $2.5\times2.5\,\mu m^2$ cases a clear uniaxial anisotropy is found superimposed on the Fe cubic anisotropy. The hard axis of this new uniaxial symmetry lies close to the [110] crystalline direction (0° in Fig. 2). For both square separations the presence of magnetic domains is clearly observable at remanence ($M_r/M_s<0.7$). These magnetic domains are more evident for $s=0.6\,\mu m$ as a result of the reduction in the square-square magnetic interaction.

B. MOKE measurements in reflected and diffracted spots

Figure 3 shows the MOKE hysteresis loops, i.e., the magnetization component parallel to the applied field, when it is applied along a hard magnetic axis (parallel to microsquare edge). The data displayed have been obtained for the $L=10\,\mu m$ array, with an interelement separation of $s=0.6\,\mu m$. The magnetic loops obtained for the reflected spot ($n=0$) show the expected shape that corresponds to an abrupt magnetization reversal.[10] When the transverse MOKE loops are recorded on the first ($n=1$), second ($n=2$), third ($n=3$), and fourth ($n=4$) horizontal diffracted spots [column (a) in Fig. 3] it is clearly observable that they are quite different from each other and also different from the one observed when the loop is recorded on the reflected spot. In principle, different shaped diffraction loops could be expected when changing the order (n) of the diffracted spot due to interference effects while magnetization reversal takes place.[11,12] It has been proposed previously that these distortions in the horizontal/vertical diffracted signals could be related to the horizontal/vertical n Fourier component of the measured projection of the magnetization in each square.[13] As a matter of fact, when the MOKE loops corresponding to the vertical diffracted spots are recorded [column (b) in Fig. 3] the differences with respect to the reflected one are less marked in comparison to the differences observed in the horizontal case. This can be explained by taking into account that magnetization inhomogeneities along the applied field direction are expected to be weaker than those produced in the direction perpendicular to the magnetic field.

In addition, as the Bragg order increases, the differences between the MO signal from diffracted and reflected spots decrease, indicating that the contributions to magnetization of high order Fourier components ($n>4$) are negligible in comparison to that produced by low order components.

Figure 3 indicates that MO measurements on the diffracted spots can be used to estimate the homogeneity of the magnetization in each Fe square. In the next section, a combination of specular and nonspecular MOT experiments will be used to determine the magnetic anisotropy constant of the different Fe squares.

C. Determination of magnetic anisotropy constants

Once the magnetic axes distribution has been determined, the MOT technique has been used to determine the magnetic anisotropy constants and to investigate their evolution with the change of L and s.

The loops shown in Fig. 3 are clear evidence of the existence of a nonhomogeneous magnetization distribution during magnetization reversal within the microsquares.[11–13] This inhomogeneous distribution is field dependent, since for high enough magnetic fields no magnetization inhomogeneities are expected. As mentioned before, MOT experiments (which provide the magnitude of magnetic anisotropy constants) require a field intensity that guarantees a single domain state during the rotation process.[4] Nevertheless, MOKE experiments on diffracted spots discussed in Sec. III B do not determine the minimum applied magnetic field that ensures the single domain state in a rotating field configuration.

In MOT experiments, the angle α between applied magnetic field and Fe easy axis is continuously changed (see Fig. 4), so that the magnetization component perpendicular to input beam polarization [$M_y=M\sin(\theta)$] also changes. In MOT experiments this component is measured as a function of the applied magnetic field angle.

Figure 5 shows the angular dependence of the intensity of the reflected (dotted lines) and first order horizontally diffracted spots (solid lines) for a $L=10\,\mu m$ array with $s=0.2$ and $s=0.6\,\mu m$ [columns (a) and (b), respectively] and for different applied magnetic field magnitudes. In all the cases zero angle corresponds to the situation where the applied magnetic field is parallel to the Fe hard axis (see Fig. 4) so that the MO signal is maximum. Note the differences between reflected ($n=0$) and diffracted ($n=1$) responses. For low magnetic fields (H=0.8 kOe) and for 90°, 270°, ...

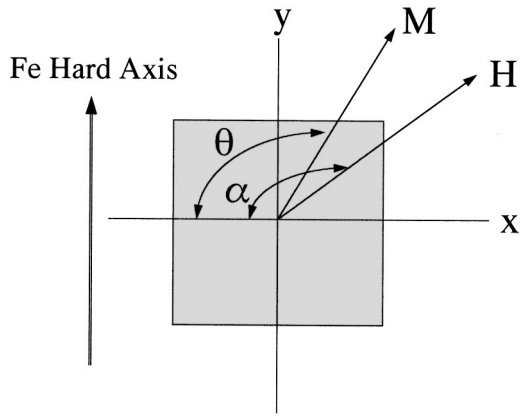

FIG. 4. Schematic of the geometrical distribution of applied magnetic field, induced magnetization, Fe hard axis, and patterned squares during MOT experiments.

angles there is a sudden increase in the diffracted intensity which is in contrast with the monotonic behavior observed in the reflected signal. The height of these peaks depends on the magnitude of the applied magnetic field. As the magnetic field increases the diffracted intensity angular dependence resembles more the reflected, or zero order, one. This similarity between specular and nonspecular MO signals indicates that an homogeneous magnetic state has been reached. This has been observed for applied magnetic fields of the order of 2 kOe. The curves obtained for $H>2$ kOe do not present remarkable differences to those shown in Fig. 5 for the $H=2.1$ kOe case. Similar experiments have been performed on the $L=2.5$ and 5 μm arrays. In all the cases we have concluded that uniform magnetic state during the whole rotation process is achieved for magnetic fields of the order of 2 kOe.

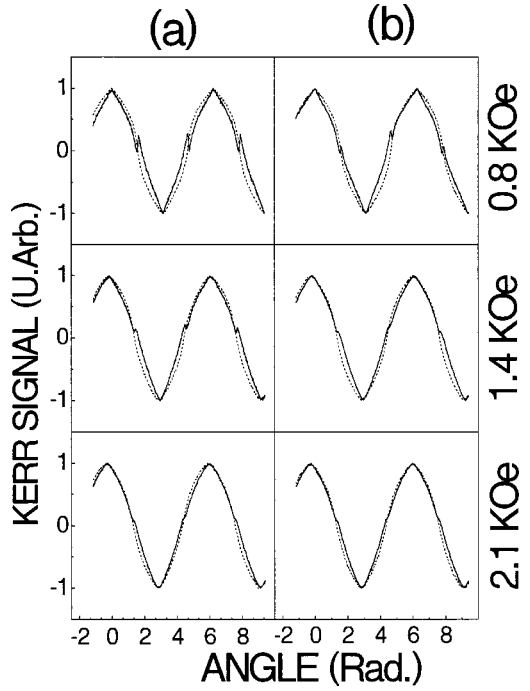

FIG. 5. MOT signal obtained from reflected (dotted line) and first order diffracted beam (solid line) as a function of applied magnetic amplitude. Data have been obtained from $L=10$ μm arrays with $s=0.2$ and 0.6 μm [columns (a) and (b), respectively].

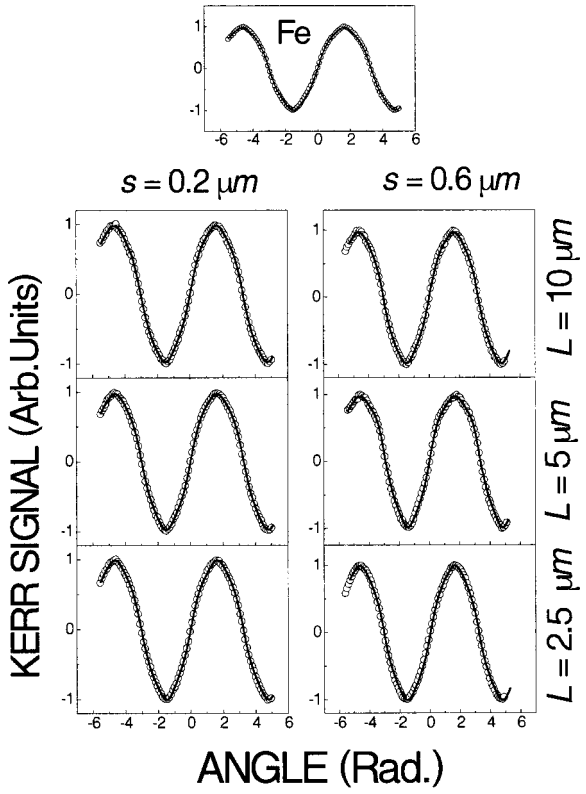

FIG. 6. Angular dependence of the reflectivity (points) and corresponding fits (lines) for square arrays with different square-square separations and periods. The continuous iron film data and fit are also shown. Applied magnetic field was 2 kOe.

When the rotating magnetic field H is applied in the plane of the film and its magnitude is high enough to guarantee a single domain state in every direction, the dependence of the reflectivity on the direction of the applied magnetic field (α) can be expressed as.[4]

$$R(\alpha)=R_0+A\cos(\theta)+B\cos^2(\theta), \tag{1}$$

where θ is the angle between the induced magnetization and the axis perpendicular to the plane of incidence (see Fig. 4). This expression is only valid in our experimental geometry where both the incident and reflected light are *p* polarized, so that only the r_{pp} reflection term contributes. Therefore the evolution of $\Delta R=R(\alpha)-R_0$ versus α represents a direct measurement of the changes in the direction of magnetization as the magnetic field rotates.

Figure 6 shows the angular dependence of ΔR for Fe continuous films as well as for the different patterns in the presence of a rotating magnetic field of 2 kOe. In the absence of any magnetic anisotropy the obtained curve would display a pure sinusoidal shape (there is no phase difference between applied magnetic field and induced magnetization). The effect of the magnetic anisotropy is to induce a phase difference between the field and the magnetization so that, in general, $\theta\neq\alpha$. When the magnetic field is rotating from an easy axis towards a hard axis the induced magnetization lags behind the field. It leads ahead when rotating from a hard axis

towards an easy one. The presence of magnetic anisotropies is then characterized by deviations from a sinusoidal reflectivity. For a single domain system the angle between applied magnetic field and induced magnetization (and therefore the shape of reflectivity versus angle curves) can be calculated minimizing the magnetic free energy. For the continuous Fe film case this can be expressed as[14]

$$E=\left(\frac{K_c}{4}\right)\sin^2 2(\theta-\beta)-HM_s\cos(\alpha-\theta-90°), \qquad (2)$$

where K_c is a cubic anisotropy constant, H the applied field, M_S the saturation magnetization, and β is the angle between the easy axis and the x axis. In our experimental conditions $\beta=45°$. The final shape of the reflectivity curve is determined by the ratio $P=K_c/2HM_S$ so that this is varied until the differences between experimental data and predicted curve are minimized. This method has been first applied to the Fe single crystalline film. The corresponding curve is shown in Fig. 6 where open circles are experimental data and the solid line is the best fit. The cubic anisotropy constant obtained from the Fe data is $K_c=4.05\times10^5$ erg cm^{-3}, which agrees with the values derived from the anisotropy field conventional hysteresis loops with H applied along a hard magnetic axis. It is also similar to values reported for Fe films of comparable thickness.[15]

To quantify the additional shape anisotropy induced by the square patterning process, the data obtained from the different square arrays are fitted by minimizing the magnetic energy of the system. In addition to the crystalline anisotropy, another term for the square shape induced anisotropy is introduced. As a first order approximation, justified by the polar plots of the reduced remanence shown in Fig. 2, this additional anisotropy has been considered as cubic for $L=10$ and 5 μm arrays so that for these cases the magnetic energy can be now written as

$$E=\left(\frac{K_{\rm sh}^c}{4}\right)\sin^2 2(\theta-\beta')+\left(\frac{K_c}{4}\right)\sin^2 2(\theta-\beta) -HM_s\cos(\alpha-\theta-90°), \qquad (3)$$

where $K_{\rm sh}^c$ is the shape anisotropy constant. The subscript c denotes that for these square arrangements this additional anisotropy corresponds to a cubic one. In expression (3) β' is the angle between the easy axis associated with the shape anisotropy and the x axis. Minimizing this free energy provides the relation between the actual angle of induced magnetization and the applied magnetic field angle. The experimental MOT curves are then fitted by keeping fixed the anisotropy constant (K_c) obtained from the continuous Fe film MOT curves. Experimental data (open circles) and best fits (solid lines) are shown in Fig. 6 for all the array configurations. In this way the fit provides the value of the shape anisotropy constant due to the square patterning. It should be noted here that the orientation of shape anisotropy easy axes (β') is also varied during the fitting procedure. The values finally obtained are $\beta'=45°\pm8°$ for all the cases, indicating that Fe easy axes and square diagonals are aligned in accordance with the patterning design. The values obtained for the shape anisotropy constants are 7.31×10^3 and 8.44×10^4 erg cm^{-3} for $s=0.6$ μm and for $L=10$ and 5 μm arrays, respectively. For 0.2 μm separation, $K_{\rm sh}$ decreases significantly down to 2.89×10^3 and 3.9×10^4 erg cm^{-3} for $L=10$ and 5 μm cases, respectively. This suggests that magnetic interactions between adjacent Fe squares become more relevant at these small separations, in good agreement with previous studies based on the analysis of hysteresis loops obtained from similar Fe square arrays.[9] Moreover, the reduction in the effective shape anisotropy for small interelement separation has been also found in MOT studies on Fe(001) stripe arrays.[4]

TABLE I. Magnetic anisotropy constants as calculated from MOT experiments as a function of array period and square-square separation. The character of the patterning induced magnetic anisotropy is also indicated for each case.

Array period (L)	Square-square separation (s) (μm)	Anisotropy constant ($\times10^4$ erg cm^{-3})	Anisotropy
10 μm	0.6	0.73	cubic
	0.2	0.28	cubic
5 μm	0.6	8.44	cubic
	0.2	3.9	cubic
2.5 μm	0.6	9.5	uniaxial
	0.2	8.9	uniaxial

For the $L=2.5$ μm arrays and in accordance with polar plots of reduced remanence, the magnetic energy of the system can be written as

$$E=(K^u)\sin^2(\theta-\beta')+\left(\frac{K_c}{4}\right)\sin^2 2(\theta-\beta)-HM_s \times\cos(\alpha-\theta-90°), \qquad (4)$$

where K^u is the uniaxial anisotropy constant and β' now determines the orientation of this uniaxial anisotropy. From the analysis of MOT curves (see Fig. 6) we have found that the corresponding easy axis is around 16° with respect to the [−110] crystalline direction in accordance to data shown in Fig. 2. In addition, the anisotropy constants obtained are 0.89×10^5 and 0.95×10^5 erg cm^{-3} for $s=0.2$ and 0.6 μm, respectively. In this case the magnetic anisotropy constant is also reduced by magnetic interaction between adjacent squares.

The values obtained for the shape anisotropy constants as a function of array period are summarized in Table I. It is clearly observable that as the square size is reduced the shape magnetic anisotropy increases, as was expected. In addition, the anisotropy constant decreases with the square-square separation due to magnetic interactions. The uniaxial anisotropy induced by the nanopatterning process in the smallest studied sizes could have different origins that are considered next.

First, any elongation along one of the sides of the squares would produce an additional uniaxial shape anisotropy. In order to analyze this possible origin, a careful determination of the square dimensions has been done by AFM experiments. They have shown that the relative elongation is as low as 5% and 2% for the $L=2.5$ μm square arrays with

$s=0.6$ and 0.2 μm, respectively, this elongation being lower than 2% for the larger squares ($L=5$ and 10 μm). This deviation from the square shape is probably related to the intensity profile of the electron-beam which could differ from a perfect Gaussian distribution. The corresponding uniaxial shape anisotropy induced in the sample plane can be estimated as

$$K_{\mathrm{ush}}=\tfrac{1}{2}(N_y-N_x)M^2, \tag{5}$$

where N_y and N_x are the demagnetizing factors along the two perpendicular in-plane directions. They can be evaluated considering the Fe (001) square elements as very flat ellipsoids, that is, their axes a, b, and c along the directions x, y, and z present the relation $a \geqslant b \gg c$. In this case the difference of the demagnetizing factors can be written as[16]

$$N_y-N_x=4\pi(c/a)\{(1-e^2)[2K(e)-E(e)] - E(e)\}/[e^2(1-e^2)^{1/2}], \tag{6}$$

where $K(e)$ and $E(e)$ are the complete elliptic integrals of the first and second kinds, respectively, and $e=[1-(b/a)^2]^{1/2}$.

Considering the upper limit for the possible induced anisotropy, that is, $b=0.95a$ (elongation of 5%), with $a=2$ μm and $c=20$ nm (Fe cube dimensions for the smallest squares), we obtain

$$K_{\mathrm{ush}}=\tfrac{1}{2}(N_y-N_x)M^2\approx 1.75\times 10^4\ \mathrm{erg\,cm^{-3}}. \tag{7}$$

This upper limit shows that, although this effect can give some contribution to the patterning induced uniaxial anisotropy, it is clearly smaller than the observed one (see Table I), so that other factors must be present.

Another effect that can contribute to the origin of the observed uniaxial anisotropy is the possible relaxation of the growth induced stresses when the film is patterned in small elements, producing a stress anisotropy. In general, this anisotropy is given by

$$K_\sigma=3/2\lambda\sigma, \tag{8}$$

where λ is the magnetostriction of the material and σ is the stress acting on the sample. Taking the experimentally observed value of the uniaxial anisotropy $K=9\times 10^4\ \mathrm{erg\,cm^{-3}}$ and $\lambda=2\times 10^{-5}$ for crystalline iron,[14] it implies internal stresses of the order of $\sigma\approx 3\times 10^9\ \mathrm{dyn\,cm^{-3}}=3\times 10^8$ Pa. On the other hand, the stress associated with an epitaxial growth in the first layers can be estimated as $\sigma_g=\tfrac{1}{2}M_Y\varepsilon$, M_Y being the Young's modulus of the material and ε the distortion produced in the lattice due to the mismatch between the substrate and the grown film. In our Fe films, $M_Y\approx 2\times 10^{11}$ Pa[17] and $\varepsilon\approx 4\%$, giving $\sigma_g\approx 4\times 10^9$ Pa. These values of σ_g are usually relaxed along the film by the formation of dislocations. However, although they are reduced, they could still become comparable with the evaluated σ needed to induce the uniaxial anisotropy as σ_g is originally one order of magnitude larger.

IV. CONCLUSIONS

We have performed a systematic investigation by magneto-optical experiments on the magnetic anisotropy characteristics of periodic arrays of Fe microsquares with different sizes and submicrometric separations. The periodic distribution of magnetic elements allows the investigation of MO response in both reflected and diffracted spots. Nonspecular measurements serve to determine when the magnetization within the microsquares reaches a homogeneous distribution. We have concluded that, if the applied field magnitude is of the order of 2 kOe, the field strength is high enough to guarantee a single domain state in a rotating field configuration.

The magnetic axes distribution has been studied by measurements of in-plane hysteresis loops at different magnetic field orientations. The magnetic anisotropy obtained depends strongly on the square size. When this is reduced below 2.5 μm, the magnetic anisotropy presents an important uniaxial character. Although some possible shape anisotropy contribution is not negligible, this uniaxial anisotropy might be mainly originated during the patterning process by the relaxation of the internal stresses of the epitaxially grown film, inducing a stress anisotropy.

Finally, we have used the MOT technique to determine the effective magnetic anisotropy constants induced by square patterning. For large square sizes, a biaxial shape anisotropy associated with the lithographed array is observed, ranging from $3\times 10^3\ \mathrm{erg\,cm^{-3}}$ to $8\times 10^4\ \mathrm{erg\,cm^{-3}}$. It decreases when the square size is reduced or the square-square separation is decreased due to the presence of magnetic interactions between neighbor elements. For the smallest squares this additional anisotropy is uniaxial, being of the order of $9\times 10^4\ \mathrm{erg\,cm^{-3}}$, which is 0.2 times the Fe crystalline constants.

ACKNOWLEDGMENTS

This work was supported by the Spanish CICYT under Contract Nos. MAT99-0724, MAT99-1063-C04-03, and MAT98-0974, and Comunidad de Madrid under Contract No. 07N/0056/1999.

[1] J. F. Smyth, S. Schultz, D. R. Fredkin, D. P. Kern, S. A. Rishton, H. Schmid, M. Cali, and T. R. Koehler, J. Appl. Phys. **69**, 5262 (1998).
[2] S. Y. Chou, Proc. IEEE **85**, 652 (1997).
[3] G. Prinz and K. Hathaway, Phys. Today **48**, 24 (1995).
[4] G. Armelles, J. L. Costa-Krämer, J. I. Martín, J. V. Anguita, and J. L. Vicent, Appl. Phys. Lett. **77**, 2039 (2000).
[5] G. A. Gibson and S. Schultz, J. Appl. Phys. **73**, 4516 (1993).
[6] O. Kitakami, T. Sakurari, and Y. Shimada, J. Appl. Phys. **79**, 6074 (1996).
[7] J. L. Costa-Krämer, J. L. Menendez, A. Cebollada, F. Briones, D. García, and A. Hernando, J. Magn. Magn. Mater. **210**, 341 (2000).
[8] J. I. Martín, Y. Jaccard, A. Hoffman, J. Nogues, J. M. George, J. L. Vicent, and I. K. Schuller, J. Appl. Phys. **84**, 411 (1998).
[9] J. L. Costa-Krämer, J. I. Martín, J. L. Menendez, A. Cebollada, J. V. Anguita, F. Briones, and J. L. Vicent, Appl. Phys. Lett. **76**, 3091 (2000).
[10] A. Anisimov, W. Platow, P. Poulopulos, M. Farle, K. Baberschke, P. Isberg, P. Granberg, and R. Wäppling, IEEE Trans. Magn. **34**, 873 (1998).
[11] P. Vavassori, V. Metlushko, R. M. Osgood, M. Grimsditch, U. Welp, G. Crabtree, W. Fan, S. R. Brueck, B. Ilic, and P. J. Hesketh, Phys. Rev. B **59**, 6337 (1999).
[12] P. Vavassori, V. Metlushko, M. Grimsditch, B. Ilic, P. Neuzil, and R. Kumar, Phys. Rev. B **61**, 5895 (2000).
[13] O. Geoffroy, D. Givord, Y. Otani, B. Pannetier, A. D. Santos, M. Schlen-

ker, and Y. Souche, J. Magn. Magn. Mater. **121**, 516 (1993).
[14] B. D. Cullity, *Introduction to Magnetic Materials* (Addison-Wesley, Reading, MA, 1972), p. 243.
[15] R. J. Hicken, S. J. Gray, A. Ercole, C. Daboo, D. J. Freeland, E. Gu, E. Ahmad, and J. A. C. Bland, Phys. Rev. B **55**, 5898 (1997).
[16] J. A. Osborn, Phys. Rev. **67**, 351 (1945).
[17] *Handbook of Chemistry and Physics*, 77th ed. (CRC, Boca Raton, FL, 1996).